# A General Design Equation for Confined Impinging Jets Mixers

**DOI:**
10.1016/j.cej.2023.142892

**Document Version**
Accepted author manuscript

# A General Design Equation for Confined Impinging Jets Mixers

M.S.C.A. Brito[1,2*], M.M. Dias [1,2], J.C.B. Lopes[3], R.J. Santos[1,2], C.P. Fonte[4*]

[1] Laboratory of Separation and Reaction Engineering – Laboratory of Catalysis and Materials (LSRE-LCM), Faculty of Engineering, University of Porto, Rua Dr. Roberto Frias, 4200-465 Porto, Portugal.

[2] ALiCE - Associate Laboratory in Chemical Engineering, Faculty of Engineering, University of Porto, Rua Dr. Roberto Frias, 4200-465 Porto, Portugal.

[3] CoLAB NET4CO2 – Network for a Sustainable CO2 Economy, Rua Dr. Júlio de Matos 828-882, 4200-355, Porto, Portugal.

[4] Department of Chemical Engineering, The University of Manchester, Oxford Road, Manchester, UK

[*]*Email: mbrito@fe.up.pt (experiments and design); claudio.fonte@manchester.ac.uk (model)*

**Abstract (maximum of 150 words)**

A General Design Equation for Confined Impinging Jets (CIJ) is proposed here, giving the prediction of the position of the opposed jets' impingement point. This equation was validated from numerical and experimental results, using fluids with viscosity ratios between 1 and 9 and density ratios between 1 and 10, both values within the industrial range of application of CIJs. The impingement point position is crucial for achieving effective mixing in CIJs, enabling the reactor's design at optimal operational conditions. The general design equation considers the stoichiometry ratio, the fluids' viscosity and density, and the reactors' dimensions. This paper also establishes a methodology for the design of working conditions and the reactor's design for the onset of the chaotic flow regime in CIJs.

**Keywords:** Mixing, Confined Impinging Jets; Computational Fluid Dynamics; Planar Laser Induced Fluorescence; Impingement Point Position; Reaction Injection Moulding.

## 1 Introduction

Confined Impinging Jets (CIJ) are highly efficient mixers that ensure the contact between two reactants injected as two opposed jets. The most challenging application of CIJ mixers is as mixing heads in Reaction Injection Moulding (RIM) machines to promote the mixing of two monomers in polymerisation reactions. CIJ mixers consist of a confined cylindrical mixing chamber with two opposed injectors and an open outlet that enables injecting the reactive mixture of monomers into a mould. A schematic drawing of CIJ mixers is shown in Figure 1a.

Effective mixing in CIJ mixers is ensured by the formation of dynamic flow structures onsetting under laminar chaotic flow regime. The operation at laminar chaotic flow regime in CIJ mixers is of the utmost importance in industrial applications, such as RIM machines, since it guarantees the full contact of both liquid streams improving the polymerisation yield in the mould (Lee, Ottino et al. 1980, Tucker and Suh 1980, Tucker and Suh 1980, Ranz 1986). Because of the high viscosity of liquid streams, turbulent regimes are generally not feasible, and the flow regime has to be laminar chaotic to promote convective mixing patterns (Brito, Esteves et al. 2018, Brito, Barbosa et al. 2022).

In RIM process, two monomers, i.e. isocyanate and polyol, are injected into a CIJ mixing chamber through two opposed jets. These monomers have quite different viscosities: isocyanate has a viscosity in the 0.1 Pa·s range, and polyols around 1 Pa·s. Mixing of isocyanate and polyol occurs in a typical CIJ mixing chamber, which has a diameter of $3 \leq D \leq 10$ mm and the injectors are 3 to 7 times smaller, i.e. $1 \leq d \leq 3$ mm (Lee, Ottino et al. 1980, Santos, Erkoç et al. 2009). These geometrical dimensions are described in Figure 1.

The high-speed injection of these monomers promotes natural flow oscillations at the collision point between both phases and the formation of vortices in each half of the mixing chamber (Wood, Hrymak et al. 1991, Santos, Erkoç et al. 2008, Shi, Li et al. 2015). These dynamic structures promote the stretching of the interface between phases in a few seconds, $t \sim 10 - 100$ ms, and the formation of lamellae of monomers, sufficiently thin for the polymerization reactions that are limited by diffusion. The mixture that leaves the CIJ mixing chamber is then discharged into a mould where most of the

polymerisation occurs. In systems with low diffusion and fast reaction, such as in polyurethane processing in RIM machines, the mixing process plays an important role in the effective performance of these devices since mixing controls the chemical reaction and thus the mechanical properties of the plastic part formed in the mould (Tucker and Suh 1980).

The huge impact of RIM technology on the chemical and automotive industries and the need for solutions that make this process more robust are the major driving forces for the extension on fundamental studies of mixing dissimilar fluids in CIJ mixers.

The issue of CIJs operation is five decades long, dating to the original CIJs patent for RIM in the 1970s (Keuerleber and Pahl 1970). Many of the papers that build up the current knowledge on CIJs are referenced in this work. The identification of flow regimes in CIJ mixers using similar fluids in both injectors has been widely reported from Planar Induced Fluorescence (PLIF), Particle Image Velocimetry (PIV) and Computational Fluid Dynamic (CFD) simulations (Lee, Ottino et al. 1980, Tucker and Suh 1980, Sandell, Macosko et al. 1983, Johnson, Wood et al. 1996, Unger, Muzzio et al. 1998, Zhao and Brodkey 1998, Zhao and Brodkey 1998, Johnson 2000, Nakamura and Brodkey 2000, Marchisio, Rivautella et al. 2006, Gavi, Marchisio et al. 2007, Gavi, Rivautella et al. 2007, Gavi, Marchisio et al. 2008, Marchisio, Omegna et al. 2008, Santos, Erkoç et al. 2008, Lince, Marchisio et al. 2009, Santos, Erkoç et al. 2009, Gavi, Marchisio et al. 2010, Icardi, Gavi et al. 2011, Fonte, Sultan et al. 2015, Fonte, Sultan et al. 2016). Brito, Barbosa et al. (2022) further studied the injection of dissimilar fluids. For both similar and dissimilar fluids, two laminar flow regimes were reported: segregated flow regime and chaotic flow regime.

In the segregated flow regime, the two liquid streams issuing from each injector leave the chamber without undergoing an effective dynamic mixing, which is promoted by the onset of vortices shedding from the opposed jets impingement point (Lee, Ottino et al. 1980, Tucker and Suh 1980, Wood, Hrymak et al. 1991, Johnson, Wood et al. 1996, Unger and Muzzio 1999, Santos, Erkoç et al. 2008). Mixing at these conditions only occurs by diffusion at the interface that coincides to the mixing chamber axis (Fonte, Sultan et al. 2015).

77 The chaotic flow regime is characterised by the disruption of the flow symmetry at the segregation plan,
78 which gives rise to the formation of a vortex street that promotes a large contact area between the liquid
79 streams (Fonte, Sultan et al. 2015). In this regime, after the injection of two high-speed jets, the two
80 fluids collide spreading radially in a squeezed fluid structure that resembles a pancake (Wood, Hrymak
81 et al. 1991). The formation of this pancake associated to the strong energy dissipation at jets' collision
82 promotes the shedding of vortices that onset natural oscillation of the jets' impingement point position.
83 The vortex street ensures the stretching of the interface between the two phases, increasing the gradient
84 concentrations and enhancing diffusion. This region is commonly called the mixing zone. Downstream,
85 fluids are further stretched by a fully developed laminar flow, having a parabolic profile, as shown in
86 Fonte, Santos et al. (2011).

87 The transition between the segregated and the self-sustainable chaotic flow regimes essentially depends
88 on the Reynolds number. For industrial application of CIJ mixers in RIM machines, the onset of the
89 chaotic flow regime has been set in a range of Reynolds number from 100 to 150, which was defined
90 for the first time by Malguarnera and Suh (1977) as

$$\mathrm{Re} = \frac{\rho v_{\mathrm{inj}} d}{\mu} \tag{1}$$

91 wherein $d$ is the diameter of injector, $v_{\mathrm{inj}}$ is the velocity at injector, $\rho$ and $\mu$ are density and viscosity,
92 respectively.

93 Fundamental studies on mixing of similar fluids defined the onset of chaotic flow regime in CIJ mixers
94 for $\mathrm{Re} > 120$. Nevertheless, Fonte et al. (2015) also observed instabilities at the interface for $103 <$
95 $\mathrm{Re} < 111$; however, this flow regime is not chaotic because vortices are not shedding from the
96 impingement point, and no oscillations of the impingement point position are observable. Therefore,
97 Fonte, Sultan et al. (2015) reported that a very large evolution on the interface's stretching rate in mixing
98 similar fluids occurs for $120 < \mathrm{Re} < 300$. For $300 < \mathrm{Re} < 600$, there is only a small evolution in
99 mixing, which usually does not compensate the decrease in the residence time in the CIJs (Nunes,
100 Santos et al. 2012). The lamellar reduction is not easily visualised for $\mathrm{Re} > 600$, due to the formation

of small eddies, typically generated in turbulent flow regimes, which cause a great homogenization of the liquids.

For a viscosity ratio between 2 and 9, Brito, Barbosa et al. (2022) reported from PLIF images that the onset of chaotic flow regime is given by the Reynolds number of the more viscous (MV) liquid stream, which must be $Re_{MV}$>150. For larger viscosity ratios, there is an increase of the Reynolds number in the less viscous (LV) liquid side. The larger Re on the LV liquid stream promotes instabilities in the MV liquid stream, which lowers the transition Reynolds number in the MV side to chaotic flow regimes. Periodic stimuli of a jet have also been shown to onset the chaotic flow regime below the transition Re values by Li, Huang et al. (2013), Shi, Li et al. (2015), Li, Wei et al. (2016).

Nevertheless, even for a Re higher than the critical one, the imbalance of jets at the impingement point position causes poor mixing, clearly shown by Fonte, Sultan et al. (2016) for similar fluids and Brito, Barbosa et al. (2022) for dissimilar fluids. The balance of opposed jets means that the opposed jets' impingement point must occur at the centre of the mixing chamber, i.e. at the mixing chamber axis (Johnson 2000, Johnson 2000, Erkoç, Santos et al. 2007, Fonte, Sultan et al. 2015, Fonte, Sultan et al. 2016, Gomes, Fonte et al. 2016). The quantification of mixing of similar fluids in Fonte, Sultan et al. (2015) clearly shows that above the critical Reynolds number, laminar mixing occurs for a flow rate ratio $r_s = 1$, which is defined by

$$r_s = \frac{\rho_1 d_1^2 v_{\mathrm{inj},1}}{\rho_2 d_2^2 v_{\mathrm{inj},2}} \tag{2}$$

where indices 1 and 2 correspond to the jet 1 and 2, according to Figure 1. When $r_s = 1$, the opposed jets with the same viscosity and density are balanced. Effective mixing is hindered by deviations from the set point of $\pm 10\%$ in the flow rate ratio. For the maximum deviation from $r_s = 1$ of 15%, the jets are completely pushed into one of the injectors, leading to clogging in industrial RIM machines due to the fast polymerisation next to the inlet nozzles. Therefore, the control of the impingement point position has a particular impact on the mixing efficiency.

For mixing fluids with different viscosities, efficient mixing occurs for conditions where the impingement point must be at the center of the mixing chamber; however, this condition does not correspond to $r_s = 1$, as for similar fluids (Brito, Barbosa et al. 2022).

Alternative techniques to make CIJ mixers operation more robust are based on the control of the static pressure difference between the opposed jets (Erkoç, Santos et al. 2007, Gomes, Fonte et al. 2016), which enables to control the jets balancing in real-time. This technology is not yet introduced in commercial RIM machines and would not overcome the limitation of mixing fluids with different flow rates.

CIJ geometry also has an impact on mixing performance. Unger and Muzzio (1999) studied two different geometries: symmetric geometry wherein both jets are injected as two opposed jets; a geometry where both injects have an angle downward at 20º; other angled backwards at 8º; and other angled forward 8º. The direct impingement of both jets only occurs in the symmetric geometry, i.e. when both injector nozzles have the same diameter. A small deviation of 1º from the injectors' axis does not ensure the industrial practice that requires the balance of the two directly opposed jets (Schütz, Piesche et al. 2005). Therefore, the directly opposed impingement of both jets is the best configuration for the highest performance in CIJ mixers because it uses all the inertia of each jet for mixing with the opposite one.

In sum, the best conditions for the most effective mixing in CIJ mixers are: *i)* directly impingement of opposed jets, making an angle of 180º between them; *ii)* both jets must operate above the critical Reynolds number, $\mathrm{Re} > 120$ for similar fluids and $\mathrm{Re}_{\mathrm{MV}} > 150$ for dissimilar fluids; and *iii)* the balance of jets, i.e. the impingement point position must be at the mixing chamber axis.

The prediction of the jets' impingement point position becomes imperative for the successful design of CIJ mixers. Malguarnera and Suh (1977) proposed that the mass flow rate must guarantee the stoichiometry for a non-unitary stoichiometry ratio. Fonte, Sultan et al. (2016) developed the elastic analogue model, which describes the impingement of jets in a CIJ mixer, taking into account the geometrical mixer parameters and the fluid physical properties of fluids. This model was already

validated for different flow rate ratios, geometrical parameters (Fonte, Sultan et al. 2016) and for a viscosity ratio between 1 and 2.

The prediction of the opposed jets impingement point position is extended in this paper to the case of dissimilar fluids comprising a viscosity ratio range between 2 and 9, which corresponds to the industrial application in RIM machines. Three models to describe the jets impingement point position are proposed, considering the direct impingement of both phases: the elastic analogue model of Fonte, Sultan et al. (2016), and two new models, which are also introduced in the following section. The validation of the model applicability for dissimilar fluids is based on 3D CFD simulations and PLIF experiments reported in Fonte, Sultan et al. (2016) for similar fluids and experimental data of Brito, Barbosa et al. (2022) for dissimilar fluids.

## 2 Analytical Models to predict Impingement Point Position

The following sections describe three analytical models: elastic analogue model; jets kinetic energy model; and jets momentum model.

### 2.1 Elastic Analogue model (EAM)

Figure 1b shows a schematic representation of the impingement of two opposed jets from the axial cut of the mixing chamber. This sketch illustrates the impingement point position in the mixing chamber. Fonte, Sultan et al. (2016) described the impingement point position assuming that the jets act as springs of equal force $F = kl$, where $k$ is the spring constant and $l$ is the spring length variation. This model is called Elastic Analogue Model (EAM). The variation of the potential energy of each jet is proportional to the jets displacement from the mixing chamber axis, $\Delta E_p = kl^2$. Thus, the potential energy of each jet is determined from the length of each jet, $l_1$ and $l_2$, as illustrated in Figure 1. The ratio of the opposed jets potential energy is proportional to the ratio of the jets kinetic energy rate, $\dot{E}_{K,1}/\dot{E}_{K,2} = l_1/l_2$, and thus the jets impingement point displacement is proportional to the kinetic energy feeding rate ratio of the opposed jets,

$$\phi_K = \frac{\rho_1 d_1^2 v_{\text{inj},1}^2}{\rho_2 d_2^2 v_{\text{inj},2}^2} \tag{3}$$

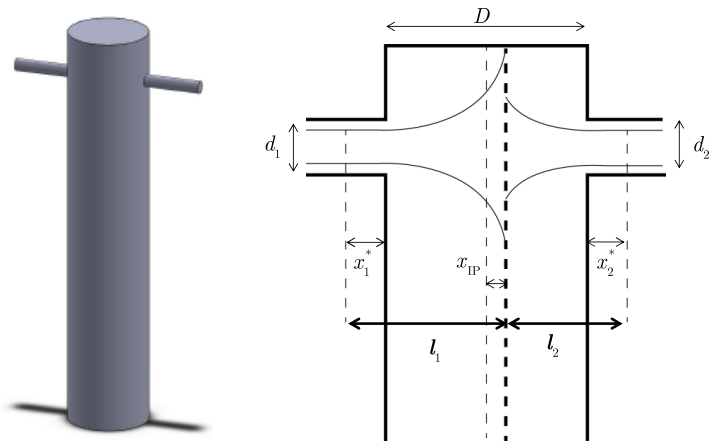


(a) (b)

Figure 1 Sketch of the impingement point in the front view CIJ mixing chamber and the respective representation of $x_1^*$, $x_2^*$, $D$, $d_1$, $d_2$, $l_1$, $l_2$ and $x_{\text{IP}}$.

Fonte, Sultan et al. (2016) introduced a correction for each jet's energy dissipation using the narrow axisymmetric jet (NAJ) model due to viscous effects. NAJ model considers that when a jet is injected in a larger expansion region from a circular hole, it remains narrow and grows slowly. It neglects the effect of the chamber walls and the additional kinetic energy dissipation due to unsteady vortex formation and detachment in the unsteady chaotic flow regime. The axial velocity of jets, according to the NAJ model (Bird, Stewart et al. 2002, White 2006) is,

$$v(x,r) = \frac{3J}{8\pi\mu x}\left[1 + \frac{1}{4}\left(\frac{C_{\text{int}} r}{x}\right)^2\right]^{-2} \tag{4}$$

where $J$ is the fed jet momentum rate, $J = (\pi/3)\rho v_{\text{inj}}^2 d^2$, $C_{\text{int}}$ is an integration constant $C_{\text{int}} = \sqrt{3\rho J/(16\pi\mu^2)}$, $r$ is the radial coordinate and $x$ is the axial coordinate. The NAJ model introduces viscosity related terms, namely the jets Reynolds numbers, in the elastic analogue model for the

prediction of the jets impingement point displacement from the mixing chamber axis, $x_{\mathrm{IP}}$ (see Figure 1). In this model, the jets impingement point position relation $(l_1/l_2)$ is given by

$$\frac{\dot{E}_{K,1}}{\dot{E}_{K,2}} = \frac{l_1}{l_2} = \frac{\int_0^\infty v_1(l_1,r)^3 2\pi\rho_1 r dr}{\int_0^\infty v_2(l_2,r)^3 2\pi\rho_2 r dr} = \sqrt{\phi_K \frac{\mathrm{Re}_1}{\mathrm{Re}_2}\frac{d_1}{d_2}} \tag{5}$$

and a momentum source is assumed, represented by $x_1^*$ and $x_2^*$ in Figure 1b, that is placed at a distance $x_i^* = \mathrm{Re_i}\, d/20$ (Fonte, Sultan et al. 2016) before the inlet,

$$\frac{D/2 + x_{IP} + x_1^*}{D/2 + x_{IP} + x_2^*} = \sqrt{\phi_K \frac{\mathrm{Re}_1}{\mathrm{Re}_2}\frac{d_1}{d_2}} \tag{6}$$

where $x_{\mathrm{IP}}$ is the jets' impingement point displacement. From the dimensionless impingement point position (shown in Figure 1b), $\xi = x_{\mathrm{IP}}/(D/2)$, and considering $x_i^* = \mathrm{Re_i}\, d/20$, Equation 5 results in

$$\xi = \frac{\sqrt{\phi_K \frac{\mathrm{Re}_1}{\mathrm{Re}_2}\frac{d_1}{d_2}}\left(1 + \frac{\mathrm{Re}_2}{10}\frac{d_2}{D}\right) - \left(1 + \frac{\mathrm{Re}_1}{10}\frac{d_1}{D}\right)}{\sqrt{\phi_K \frac{\mathrm{Re}_1}{\mathrm{Re}_2}\frac{d_1}{d_2}} + 1} \tag{7}$$

where $\xi$ can take values from -1 to 1 since the jets are bounded by walls and cannot expand up to the position of the momentum source points, which are placed inside the injectors.

Equation 7 enables the design of CIJ mixers for mixing at non-unitary flow rate ratios, $r_s \neq 1$, by changing the diameter of the nozzles guaranteeing the balance of jets for $\xi = 0$. The full derivation of EAM, the validation, and the application to the design of CIJ mixers with $r_s \neq 1$ for similar fluids was reported in Fonte, Sultan et al. (2016).

The elastic analogue model, Equation 7, takes into account the differences in the fluid viscosities, indicating that the viscosity also plays a role in the jets' equilibrium condition. The differences in viscosities are taken into account in the Reynolds number term ($\mathrm{Re}_1$ and $\mathrm{Re}_2$) of Equation (7). The model was validated for different flow rates considering equal viscosity in the two inlet jets.

## 2.2 Jets Kinetic energy model (KEM)

A new model is introduced for the description of the impingement point position in CIJ mixing chambers. This model considers that the kinetic energy of both jets at the impingement point (at $r = 0$ and $l = [l_1, l_2]$) is balanced. Hereupon, the equilibrium between the kinetic energy at the impingement point is determined considering a Lagrangian entity belonging to each jet,

$$\rho_1 v_1^2(l_1, r = 0) = \rho_2 v_2^2(l_2, r = 0) \tag{8}$$

where $v_1$ and $v_2$ are the velocities of jets 1 and 2 at the impingement point position described by the NAJ model (Equation (4)). The point source of momentum assumed by the NAJ model corresponds to the position in the injector where the axial velocity, $v(x, r = 0)$, is equal to the maximum velocity achieved in the injector. Considering a fully developed parallel parabolic velocity profile along the injectors and equalising to the NAJ model, the point source is $x_i^* = \mathrm{Re}_i\, d/16$.

Replacing $v_1(l_1, r = 0)$ and $v_2(l_2, r = 0)$ by the NAJ model in Equation (8), it results in

$$\rho_1 \left(\frac{3J_1}{8\pi\mu_1 l_1}\right)^2 = \rho_2 \left(\frac{3J_2}{8\pi\mu_2 l_2}\right)^2 \tag{9}$$

According to Figure 1, the expression for each jet length, $l_1$ and $l_2$, can be rewritten as a function of the momentum sources, $x_1^*$ and $x_2^*$, and the impingement point position, $x_{\mathrm{IP}}$, as

$$\begin{cases} l_1 = x_1^* + \dfrac{D}{2} + x_{\mathrm{IP}} \\ l_2 = x_2^* + \dfrac{D}{2} - x_{\mathrm{IP}} \end{cases} \tag{10}$$

The jet lengths can be rewritten in Equation (9) according to Equation (10), where $x_1^*$ and $x_2^*$ are the source points given by $x_i^* = \mathrm{Re}_i\, d/16$,

$$\frac{\rho_1^{1/2} J_1}{\mu_1 \left(\frac{D}{2} + x_{\mathrm{IP}} + \frac{\mathrm{Re}_1 d_1}{16}\right)} = \frac{\rho_2^{1/2} J_2}{\mu_2 \left(\frac{D}{2} + x_{\mathrm{IP}} + \frac{\mathrm{Re}_2 d_2}{16}\right)} \tag{11}$$

From Equation (11), a dimensionless impingement point position $\xi = x_{\mathrm{IP}}/(D/2)$ can be estimated according to

$$\xi = \frac{\left[\frac{\rho_1^{1/2}}{\rho_2^{1/2}}\phi_M\frac{\mu_2}{\mu_1}\right]\left(1+\frac{Re_2}{8}\frac{d_2}{D}\right)-\left(1+\frac{Re_1}{8}\frac{d_1}{D}\right)}{\frac{\rho_1^{1/2}}{\rho_2^{1/2}}\phi_M\frac{\mu_2}{\mu_1}+1} \quad (12)$$

where $\phi_M = J_1/J_2$ is the jets' momentum rate ratio.

The kinetic energy model described in Equation (12) considers that the impingement point position is fully described by the balance of kinetic energy of two passive particles at the jets contact point. This model also accounts for the fluids' viscosities, considered in $\mathrm{Re}_1$ and $\mathrm{Re}_2$, and the geometrical parameters of CIJ mixers. The main difference between the elastic analogue model and kinetic energy model stems from the fact that the first one assumes the balance of the kinetic energy rate of both jets from an analogy to two springs. In contrast, the second one refers to the equilibrium of the kinetic energy from two particles at the impact point position.

### 2.3 Jets momentum model (MM)

A new approach is also introduced for the prediction of the impingement point position. The momentum model is based on the balance of the linear momentum of two particles, issued from opposed jets, at the impingement point, i.e. at $r = 0$ and $l = [l_1, l_2]$. This balance is described by

$$\rho_1 v_1(l_1, r = 0) = \rho_2 v_2(l_2, r = 0) \quad (13)$$

where $v_1$ and $v_2$ are predicted by the NAJ model (Equation (4)), enabling to rewrite Equation (13) as

$$\rho_1\left(\frac{3J_1}{8\pi\mu_1 l_1}\right) = \rho_2\left(\frac{3J_2}{8\pi\mu_2 l_2}\right) \quad (14)$$

The dimensionless impingement position, $\xi = x_{\mathrm{IP}}/(D/2)$, can be estimated by

$$\xi = \frac{\left[\frac{\rho_1}{\rho_2}\phi_M\frac{\mu_2}{\mu_2}\right]\left(1+\frac{Re_2}{8}\frac{d_2}{D}\right)-\left(1+\frac{Re_1}{8}\frac{d_1}{D}\right)}{\frac{\rho_1}{\rho_2}\phi_M\frac{\mu_2}{\mu_1}+1} \quad (15)$$

The momentum model described in Equation (15) predicts the impingement point from the balance of the linear momentum of a Lagrangian entity belonging to each jet at the impingement point position.

The difference between the kinetic energy model (Equation (12)) and the momentum model (Equation (15)) is in the density ratio term. In Equation (12), the term is $\sqrt{\rho_1/\rho_2}$ while, in Equation (15), this term is $\rho_1/\rho_2$. Therefore, the validation of models is only verified for high-density ratios. A sensibility analysis of the three models is presented in this paper enabling the validity range for each one.

## 3 Validation of models from experimental and numerical results

Experimental and CFD results of mixing of liquids with a viscosity ratio of 1 are reported in Fonte, Sultan et al. (2015), while for dissimilar fluids with a viscosity ratio range between 2 and 9, results are in Brito, Esteves et al. (2018) and Brito, Barbosa et al. (2022). Experiments were run in a transparent CIJ mixer, which enables the visualization of the flow inside the mixing chamber. A laser sheet illuminates a plan of the mixing chamber, cutting it through the injectors. Liquid streams were injected through the opposed jets. One of the fluids was dyed with Rhodamine 6G, and the other was a clear liquid. The doped fluid is fluorescent, enabling to capture PLIF image that maps the tracer. A fully description of PLIF experiments is described in Brito, Esteves et al. (2018), Brito, Barbosa et al. (2022). CFD simulations were run using ANSYS Fluent to solve continuity, Navier-Stokes and Species equations for the mixing of dissimilar fluids.

Tables 1 and 2 summarise the dimensions of mixing chambers and the working conditions considered for the models' validation, respectively. The experimental and numerical results to validate the models in Figures 2-8 are reported in Fonte, Sultan et al. (2016) and Brito, Barbosa et al. (2022). CFD and experimental studies identified the flow regimes in symmetric and asymmetric mixing chambers, i.e. for reactors with equal and different nozzles' diameters. The three models proposed in this work, only differ when the physical properties of the fluids are dissimilar. So, for similar fluids, they all stand valid as proven for the EAM in Fonte, Sultan et al. (2016), as it will be shown later.

The jets' impingement point position can be measured from PLIF experiments and CFD results. The point where both jets collide was determined from CFD results of the axial velocity profile along the injectors axis. The jets' impingement position corresponds to the stagnation point of the axial velocity, $v(x_{\mathrm{IP},} r = 0) = 0$. The $\xi$ value is also determined from PLIF images plotting the value of the color at

each pixel along the line defined from the injectors' axes. Therefore, both jets' contact points are marked by a steep gradient in this plot. The impingement point position at each condition was determined from an average of 10 PLIF contour maps.

Table 1. CIJ Geometries under analysis in this paper.

| **Chamber #** | $\boldsymbol{D}$ **( m)** | $\boldsymbol{d_1}$ **( m)** | $\boldsymbol{d_2}$ **( m)** |
|---|---|---|---|
| 1 | 10 | 1.5 | 1.5 |
| 2 | 10 | 1.5 | 1.9 |

For mixing similar fluids, EAM has already been validated by Fonte, Sultan et al. (2016), and a good agreement between this model, experimental and numerical data is achieved. The validity of KEM and MM for similar conditions is examined here. Figure 2 shows the dimensionless impinging point in the mixing chamber for mixing of similar fluids, $\mu_1 = \mu_2 = 20$ mPa · s, at $\mathrm{Re}_1 = 50$. In Figure 2a, the experiments were run in Chamber 1, where $d_1 = d_2 = 1.5$ mm, and in Figure 2b, the experiments were run in a chamber where $d_1 = 1.9$ mm and $d_2 = 1.5$ mm, i.e. with the same dimensions of Chamber 2 (Table 1), but mirrored. PIV and CFD results in Figure 2 were reported by Fonte, Sultan et al. (2016) and used to compare both models. Very slight differences between both models are registered for similar fluids, meaning that EAM, KEM and MM can be used to design CIJ mixers working with similar fluids.

Further EAM, KEM and MM validation is made for viscosity ratios larger than unity. Figure 3 and Figure 4 show the plots of the normalised displacement of the jets impingement point from the mixing chamber axis, $\xi$, for Chamber 1 and $\mu_1/\mu_2 = 2$, as a function of the jets kinetic energy rate ratio, $\phi_K$, in Figure 3a and Figure 4a, and as a function $\mathrm{Re}_2$ in Figure 3b and Figure 4b. In Figure 3, the Reynolds number at jet 1 was set at $\mathrm{Re}_1 = 50$ and in Figure 4 at $\mathrm{Re}_1 = 100$. These plots clearly show that the position of jets is extremely sensitive to $\phi_K$ , and the balancing condition is no longer at $\phi_K = 1$. This is affected by the fact that $\mathrm{Re}_1 \neq \mathrm{Re}_2$ at the equilibrium conditions, as shown in Figures 3b and 4b, that slightly offsets the conditions for $\xi = 0$.

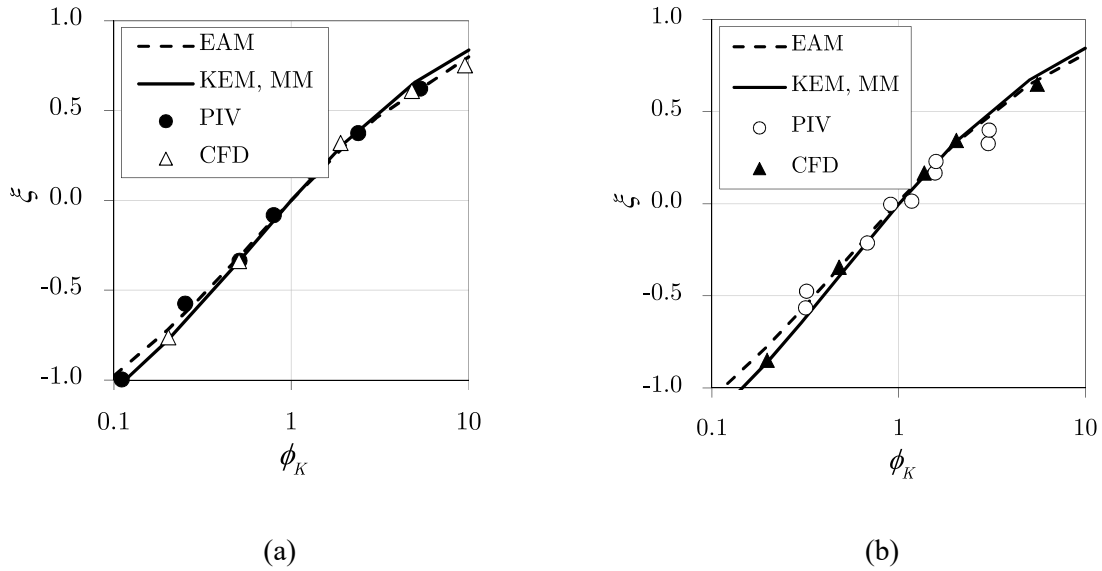


288 Figure 2. Non-dimensional impingement point position from the elastic analogue model (EAM), kinetic energy
289 model (KEM), momentum model ( MM), CFD results from Fonte, Sultan et al. (2016) and PIV data from Fonte,
290 Sultan et al. (2016) as a function of the jets kinetic energy rate for similar fluids at $\mathrm{Re}_1 = 50$ and using (a)
291 Chamber 1 and (b) mirrored Chamber 2.

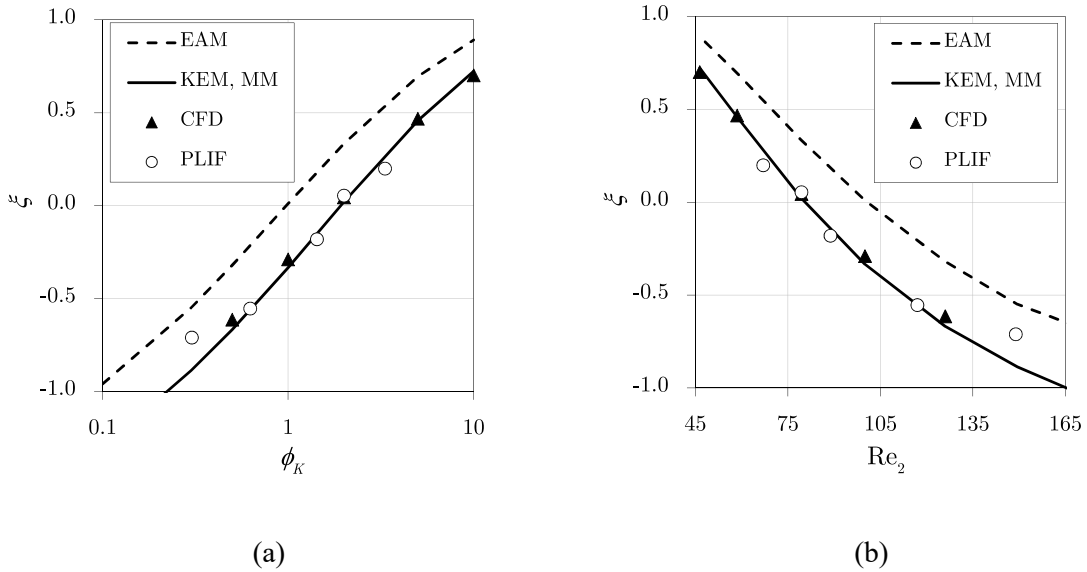


292 Figure 3. Non-dimensional impingement point position from the elastic analogue model (EAM), kinetic energy
293 model (KEM), momentum model ( MM) , CFD results and PLIF data from Brito, Barbosa et al. (2022) for
294 mixing of fluids with a viscosity ratio 2:1, $\mu_1 = 40$ mPa · s and $\mu_2 = 20$ mPa · s at $\mathrm{Re}_1 = 50$ and using
295 Chamber 1 versus (a) the jets' kinetic energy rate; (b) the Reynolds number at jet 2.

Figures 3 and 4 give a comparison between the three models (EAM, KEM and MM), and CFD and PLIF data. The position of the impingement point for a viscosity ratio $\mu_1/\mu_2 = 2$ is clearly better described from the balance of kinetic energy (Equation (12)) and the linear momentum (Equation (15)) than by EAM, particularly in this validity range $0.1 < \phi_K < 10$. The predictions of $\xi$ given by KEM and MM are coincident because CIJ mixer is operating at symmetric flow conditions in terms of density ratios. KEM and MM models only differ for cases where the fluids have different densities, $\rho_1 \neq \rho_2$.

Figure 4 shows that the fitting of KEM and MM to the experimental data is not as good as for CFD results. This may be caused by the flow rate ratio deviation during the experimental running, which can lead to a deviation of up to 30 % in $\phi_K$. However, since CFD simulation results, KEM and MM are completely coincident, these models can be validated as a design tool for these working conditions. The complete validation of this CFD data and comparison with the experiments is made in Brito, Barbosa et al. (2022).

Figure 5 shows the fitting of KEM and MM to PLIF and CFD data, providing experimental and numerical validation of these models for mixing of fluids with a viscosity ratio $\mu_1/\mu_2 = 1/5$ in Chamber 1, namely at $\mathrm{Re}_2 = 50$. On the other hand, EAM does not predict the displacement of the impingement point in the mixing chamber, showing an even larger deviation than for $\mu_1/\mu_2 = 2$. Furthermore, in Figures 3 and 4, EAM overpredicts PLIF and CFD data, while in Figure 5, this model underpredicts the results. This involves the definition of the injection of fluids in CIJ mixer. For viscosity $\mu_1/\mu_2 = 2$, MV fluid is injected through jet 1, and for viscosity $\mu_1/\mu_2 = 1/5$, the corresponding stream is delivered through jet 2. The description of the jets' balancing provided by EAM is deteriorating with the viscosity ratio.

In addition, conditions under analysis in Figure 5 consider that the density ratio of streams is $\rho_1/\rho_2 \sim 1$, and so KEM and MM give the same description of $\xi$. The validation of KEM and MM from PLIF and CFD results estimates the conditions for $\xi = 0$, at $\mathrm{Re}_1 = 165$ and $\mathrm{Re}_2 = 50$, according to Figure 5b.

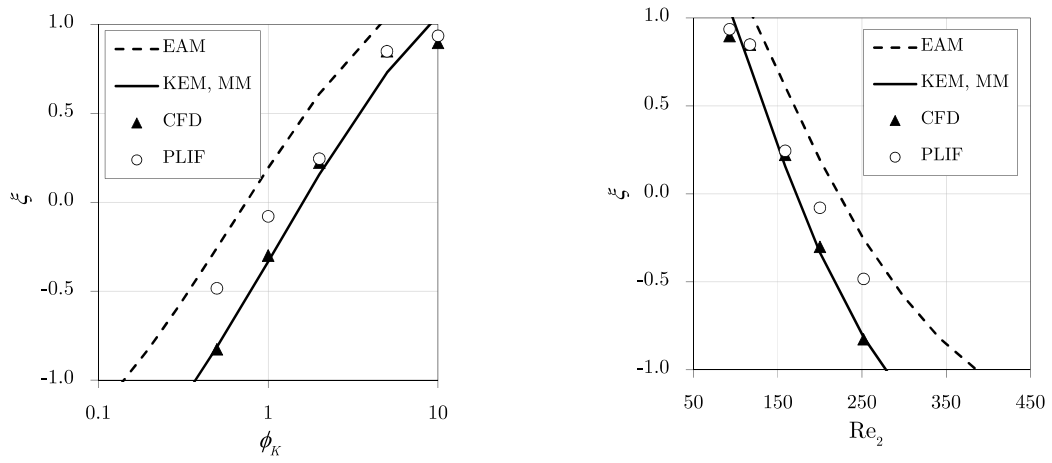


(a) (b)

Figure 4. Non-dimensional impingement point position from the elastic analogue model (EAM), kinetic energy model (EAM), momentum model ( MM), CFD results and PLIF data from Brito, Barbosa et al. (2022) for mixing of fluids fluids with a viscosity ratio 2:1, $\mu_1 = 40$ mPa · s and $\mu_2 = 20$ mPa · s at $\mathrm{Re}_1 = 100$ and using Chamber 1 versus (a) the jets' kinetic energy rate; (b) the Reynolds number at jet 2.

EAM, KEM and MM also take into account the geometrical parameters of CIJ mixing chamber. Validation of these models was then extended to the asymmetric mixing chamber, Chamber 2, where $d_1/d_2 = 1.5/1.9$. Figure 6 shows the impingement point position described by EAM, KEM, MM, CFD simulations and PLIF data for $\mathrm{Re}_2 = 45$ when two fluids with a viscosity ratio $\mu_1/\mu_2 = 1/5$ are mixed in Chamber 2. PLIF experiments corroborate the CFD results and provide validation of the ability of KEM and MM to predict the contact point of jets in chambers with different diameters. Once again, the similarities between KEM and MM result from the unity of density ratio of streams, $\rho_1/\rho_2 \sim 1$, making both expressions (Equations (12) and (15)) numerically equal.

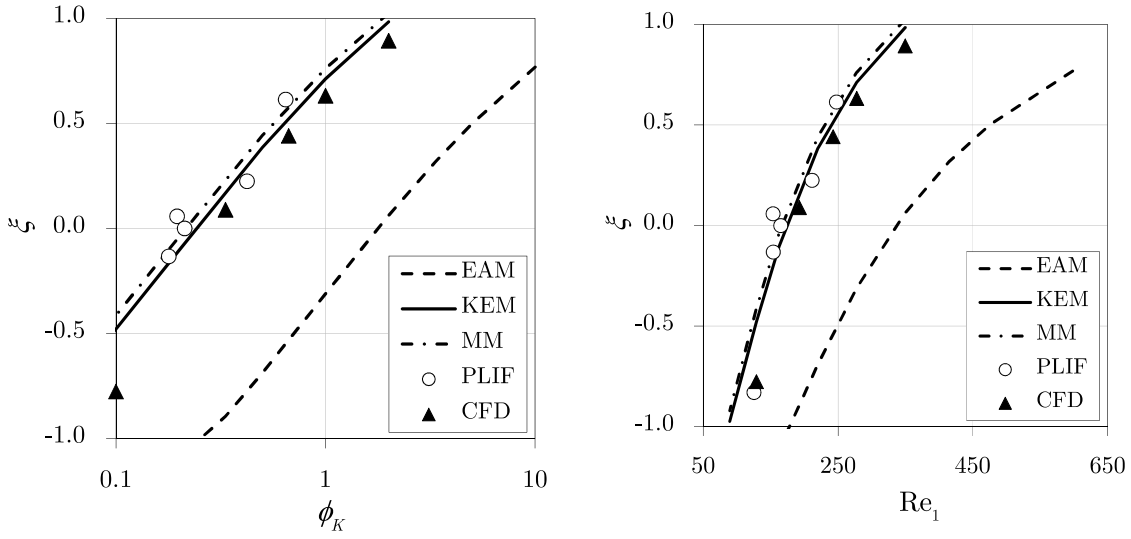


(a) (b)

Figure 5. Non-dimensional impingement point position from the elastic analogue model (EAM), kinetic energy model (KEM), momentum model ( MM), CFD results and PLIF data from Brito, Barbosa et al. (2022) for mixing of fluids fluids with a viscosity ratio 1:5, $\mu_1 = 9.2\ \mathrm{mPa \cdot s}$ and $\mu_2 = 47.8\ \mathrm{mPa \cdot s}$ at $\mathrm{Re}_2 = 50$ and using Chamber 1 versus (a) the jets' kinetic energy rate; (b) the Reynolds number at jet 1.

Small deviations exist in the numerical and experimental data from KEM and MM. These small deviations can be caused due to the simplification of the models since NAJ model is assumed. On the other hand, PLIF-based measurements are prone to uncertainties to fluctuations in light intensity, small differences in the refractive index of the two fluids injected, and limitations in the determination of the impingement point position from the plot of colors. However, Figure 6 clearly shows that data is adjusted from these models with an accuracy that falls below the experimental one. The elastic analogue model for the non-unitary viscosity ratios, $\mu_1/\mu_2 \neq 1$, cannot make a good prediction of the impingement point position. Figure 6b also shows that the working conditions for the central position of the impingement point position are at $\mathrm{Re}_1 = 165$ and $\mathrm{Re}_2 = 45$.

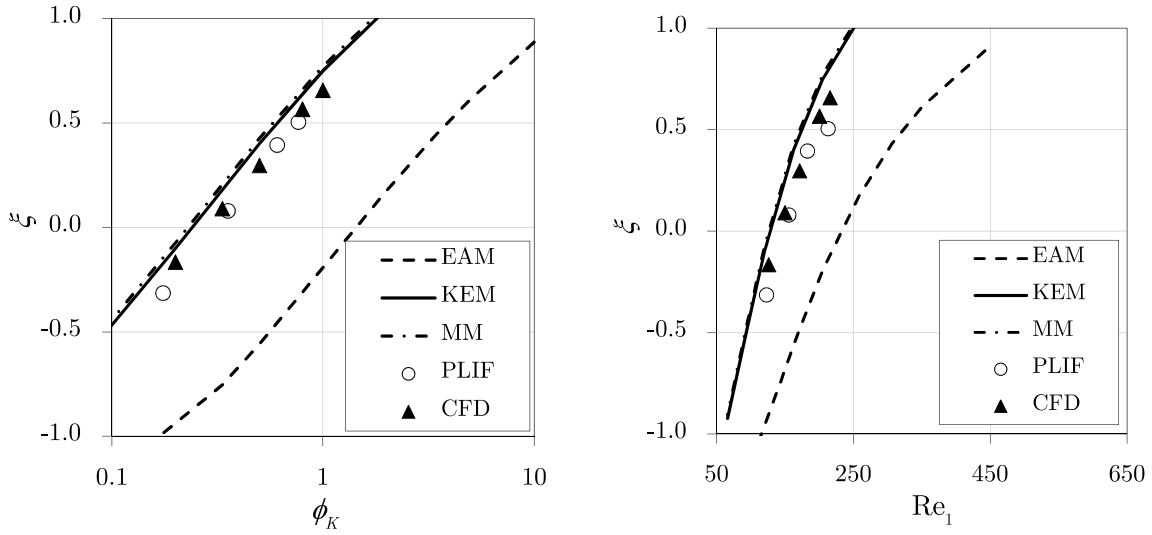


(a) (b)

Figure 6. Non-dimensional impingement point position from the elastic analogue model (EAM), kinetic energy model (KEM), momentum model ( MM), CFD results and PLIF data from Brito, Barbosa et al. (2022) for mixing of fluids with a viscosity ratio 1:5, $\mu_1 = 9.5\ \mathrm{mPa \cdot s}$ and $\mu_2 = 48\ \mathrm{mPa \cdot s}$ at $\mathrm{Re}_2 = 45$ and using Chamber 2 versus (a) the jets' kinetic energy rate; (b) the Reynolds number at jet 1.

Figure 7 displays the impingement point position as a function of $\phi_K$ and Re of jet 1 for mixing of two streams with a viscosity ratio $\mu_1/\mu_2 = 1/9$, $\mu_1 = 9.1\ \mathrm{mPa \cdot s}$ and $\mu_2 = 81.1\ \mathrm{mPa \cdot s}$ at $\mathrm{Re}_2 = 45$ in Chamber 1. KEM and MM are approximately coincident and predict PLIF and CFD data. The same is not observed for EAM. The impingement point at $\phi_K = 1$ is no longer coincident with the mixing chamber axis and, the balance of jets at the centre of the chamber occurs at $\mathrm{Re}_1 = 200$ and $\mathrm{Re}_2 = 45$, as shown in Figure 7b.

These results (from Figures 2 to 7) provide clear evidence that KEM and MM should be used for viscosity ratios larger than unity. EAM is valid for similar fluids and for symmetric or asymmetric mixing chambers (Fonte, Sultan et al. 2016). Nevertheless, the working conditions studied are not sufficient to demonstrate the differences between KEM and MM. The full validation of the best prediction of impingement point requires the simulation of an extreme condition for high-density ratio, enabling the distinction of both models. Although these conditions do not have an envisioned industrial application, 3D CFD simulations were performed for a density ratio $\rho_1/\rho_2 = 1/10$, a viscosity ratio of

$\mu_1/\mu_2 = 1/5$ and using an asymmetric CIJ mixing chamber, $d_1 \neq d_2$.The Reynolds number at jet 1 was set as constant, $\mathrm{Re}_2 = 45$.

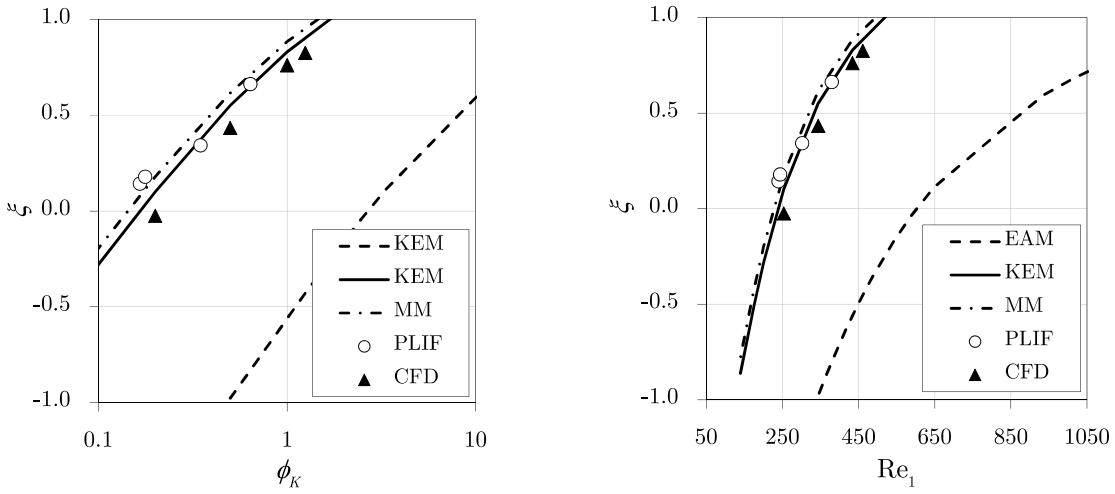


(a) (b)

Figure 7. Non-dimensional impingement point position from the elastic analogue model (EAM), kinetic energy model (KEM), momentum model ( MM), CFD results and PLIF data from Brito, Barbosa et al. (2022) for mixing of fluid with a viscosity ratio 1:9, $\mu_1 = 9.1\ \mathrm{mPa \cdot s}$ and $\mu_2 = 81.1\ \mathrm{mPa \cdot s}$ at $\mathrm{Re}_2 = 45$ and using Chamber 1 versus (a) the jets' kinetic energy rate; (b) the Reynolds number at jet 1.

CFD working conditions of this extreme case were the same as previously described in Brito, Barbosa et al. (2022). A parabolic velocity profile, normal to each injector, was defined at each inlet through a User Defined Function (UDF). No slip conditions were set at the walls, a uniform pressure value was set at the outlet, and the geometry was discretised with a hexahedral mesh of $2 \times 10^6$ nodes. The continuity and Navier Stokes equations were solved using ANSYS Fluent package. The mass transfer between the two fluids was simulated from the convection-diffusion equation, considering a molecular diffusivity of $D_m = 10^{-9}\ \mathrm{m^2\ s^{-1}}$. Simulations were run at steady state; a pressure-based solver was used with SIMPLEC pressure-velocity coupling scheme and, for the spatial discretisation, Second Order UPWIND.

Figure 8 shows the impingement point position as a function of jets' kinetic energy (Figure 8a) and Reynolds number at jet 1 (Figure 8b). The difference in densities shows that KEM is the model that

best predicts experimental and CFD data. This means that the shifting of the impingement point in CIJ mixer is exclusively given by the kinetic energy balance at the contact point between jets.

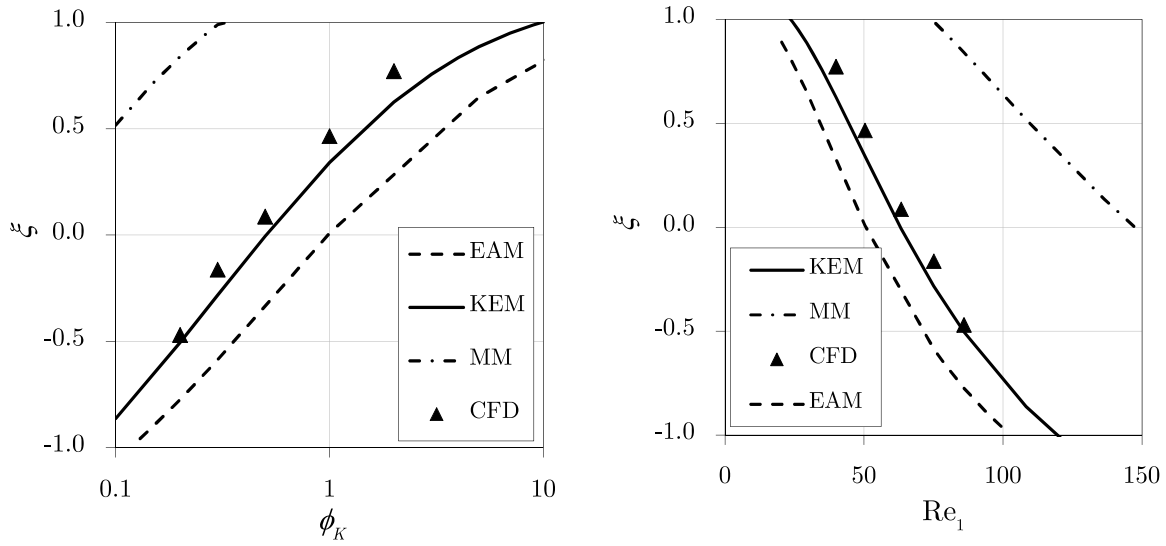


(a) (b)

Figure 8. Non-dimensional impingement point position from the elastic analogue model (EAM), kinetic energy model (KEM), momentum model ( MM) , CFD results and PLIF data for mixing of fluid with a viscosity ratio 1:5, $\mu_1 = 9.5\ \mathrm{mPa \cdot s}$ and $\mu_2 = 48\ \mathrm{mPa \cdot s}$, and densities $\rho_1 = 100\ \mathrm{kg\ m^{-3}}$ and $\rho_1 = 1000\ \mathrm{kg\ m^{-3}}$, at $\mathrm{Re}_2 = 45$ and using Chamber 2 versus (a) the jets' kinetic energy rate; (b) the Reynolds number at jet 2.

Table 2 summarises the models that described each working condition studied in this paper. These results were validated in a particular range of a viscosity ratio from 1 to 9 and a density ratio from 1 to 10. EAM only fits the experimental and numerical results for similar fluids. This indicates that the balance of kinetic energy fluxes of opposed jets is not the necessary condition to define the central position of jets impingement point. MM predicts the tendency and the actual position of the jets impingement point for similar fluids and fluids with different viscosities and similar densities. However, for high-density ratios, MM does not describe $\xi$. KEM fully predicts the impingement point position, ensuring a good prediction for similar and dissimilar fluids using asymmetric mixing chambers, and therefore hereafter, this model constitutes a General Design Equation (GDE) for CIJs.

Table 2 Summary of the validity range of each model.

| Case # | $\mu_1/\mu_2$ | Physical Properties | Chamber | Models |
|---|---|---|---|---|
| 1 | 1 | $\mu_{LV} = 20\ \text{mPa}\cdot\text{s};\ \rho_{LV} = 1000\ \text{kg m}^{-3}$<br>$\mu_{MV} = 20\ \text{mPa}\cdot\text{s};\ \rho_{MV} = 1000\ \text{kg m}^{-3}$ | 1; 2 | EAM, KEM, MM |
| 2 | 2 | $\mu_{LV} = 20\ \text{mPa}\cdot\text{s};\ \rho_{LV} = 1000\ \text{kg m}^{-3}$<br>$\mu_{MV} = 40\ \text{mPa}\cdot\text{s};\ \rho_{MV} = 1000\ \text{kg m}^{-3}$ | 1 | KEM, MM |
| 3 | 2 | $\mu_{LV} = 20\ \text{mPa}\cdot\text{s};\ \rho_{LV} = 1000\ \text{kg m}^{-3}$<br>$\mu_{MV} = 40\ \text{mPa}\cdot\text{s};\ \rho_{MV} = 1000\ \text{kg m}^{-3}$ | 2 | KEM, MM |
| 4 | 1/5 | $\mu_{LV} = 9.2\ \text{mPa}\cdot\text{s};\ \rho_{LV} = 1339\ \text{kg m}^{-3}$<br>$\mu_{MV} = 47.8\ \text{mPa}\cdot\text{s};\ \rho_{MV} = 1215\ \text{kg m}^{-3}$ | 1 | KEM, MM |
| 5 | 1/5 | $\mu_{LV} = 9.5\ \text{mPa}\cdot\text{s};\ \rho_{LV} = 1339\ \text{kg m}^{-3}$<br>$\mu_{MV} = 48.0\ \text{mPa}\cdot\text{s};\ \rho_{MV} = 1285\ \text{kg m}^{-3}$ | 2 | KEM, MM |
| 6 | 1/9 | $\mu_{LV} = 9.1\ \text{mPa}\cdot\text{s};\ \rho_{LV} = 1371\ \text{kg m}^{-3}$<br>$\mu_{MV} = 81.1\ \text{mPa}\cdot\text{s};\ \rho_{MV} = 1217\ \text{kg m}^{-3}$ | 1 | KEM, MM |
| 7 | 1/5 | $\mu_{LV} = 9.5\ \text{mPa}\cdot\text{s};\ \rho_{LV} = 100\ \text{kg m}^{-3}$<br>$\mu_{MV} = 48.0\ \text{mPa}\cdot\text{s};\ \rho_{MV} = 1000\ \text{kg m}^{-3}$ | 2 | KEM |

This model describes the impingement point position in CIJs that is relevant for the design of these mixers. This model was validated using fluids with viscosity ratios between 1 and 9 and density ratios between 1 and 10, which limits the implementation of this model to industrial applications. The model also has some simplifications regarding interfacial tension, the impact of surrounding walls, to name a

few. So, after the first approach to this model, the CIJ design should be validated with CFD simulations comprising a more comprehensive description of each process physics.

The studied validation range partially describes the industrial applications of CIJ mixer considered in this paper. In PU-RIM processing, a typical polyol has a viscosity in the range of $\mu = 1\ \mathrm{Pa \cdot s}$ and a density $\rho = 1000\ \mathrm{kg\ m^{-3}}$ and a generic isocyanate has $\mu = 0.1\ \mathrm{Pa \cdot s}$ and $\rho = 1000\ \mathrm{kg\ m^{-3}}$, i.e. a viscosity ratio $\mu_1/\mu_2 \sim 10$ and a density ratio $\rho_1/\rho_2 \sim 1$.

## 4 Process Design of CIJ mixers

The validation of GDE assesses the full control of the impinging point position in the CIJ mixing chamber. The robust methodology proposed in this work to design processes in CIJ mixers gives a potentially very significant contribution to research and industry. On the research side, GDE will avoid, or even solve problems in pilot RIM machines and will ensure the best mixing conditions for research on materials processing with CIJs. Inefficient mixing usually increases manufacturing costs due to the unsuccessful achievement of final product requirements. For instance, in RIM technology, the mixing flaws cause wet-spots of unreacted monomers in the injected parts leading to high rejection rates. On the other hand, incorrect design of experiments can also cause operational problems. For example, in processing polyurethanes (PU) in RIM machines, the imbalance flow conditions can cause clogging problems in the nozzle due to the formation of polymer closer or even inside of one inlet. The sate-of-art in RIM to avoid operational conditions is the use of flow restrictors at the mixing head, which largely increases the power of fluid metering components. Furthermore, these flow restrictors need to be tuned on a case-by-case basis. GDE offers new routes for the design of mixing heads adapted to each formulation, without the need for tuning (Lopes, Santos et al. 2013).

The design of experiments in CIJs, according to the results of this paper, must be done considering stoichiometry; therefore, the nozzle diameters must be designed from GDE, as described in Figure 9. GDE takes into account the geometrical parameters and the physical properties of both liquid streams. The design of experiments involving dissimilar fluids in CIJ mixer must take into account the critical conditions for effective mixing: the jets have to be balanced, i.e. $\xi = 0$, and the Reynolds number of

427 the more viscous fluid must be above the critical value ($\mathrm{Re_{MV}} > 150$). Therefore, experiments can be
428 designed following the flowchart shown in Figure 9, which results in

$$\sqrt{\frac{\rho_2}{\rho_1}}\, r_s \frac{\mathrm{Re}_1}{\mathrm{Re}_2}\frac{d_2}{d_1} = \frac{8D + \mathrm{Re}_1 d_1}{8D + \mathrm{Re}_2 d_2} \tag{16}$$

429 PU processing is here described as the case study for the design of CIJ mixers. Considering a polyol
430 with $\mu = 0.6\ \mathrm{Pa \cdot s}$ and $\rho = 900\ \mathrm{kg\ m^{-3}}$ and a generic isocyanate with $\mu = 0.2\ \mathrm{Pa \cdot s}$ and $\rho =$
431 $1230\ \mathrm{kg\ m^{-3}}$, the CIJ geometry was designed from GDE considering the impingement of both jets at
432 the mixing chamber, $\xi = 0$, and the Reynolds number of both jets is above the critical, $\mathrm{Re} > 150$.
433 Figure 10 shows the results for different stoichiometric ratios, i.e. $r_s =$
434 [0.5; 0.75; 1; 1.25; 1.5; 1.75; 2], where $r_s$ is defined by Equation (1). Results in Figure 10 were
435 determined from a system of three equations: Equation (16), Equation (2) and Equation (1) for $\mathrm{Re}_2$.
436 The Reynolds number of isocyanate was kept constant, $\mathrm{Re_I} = 160$, and the Reynolds number of polyol
437 was changed for different nozzle diameters and flow rates. The black curves in Figure 10 correspond to
438 the nozzle diameters through where polyol is injected; the grey curve is the diameter of isocyanate jet
439 and $\mathrm{Re_P}$ is the Reynolds number of polyol stream. Figure 10 is an example of the implementation of
440 GDE as a design tool to the design CIJ mixing chambers for RIM processes.

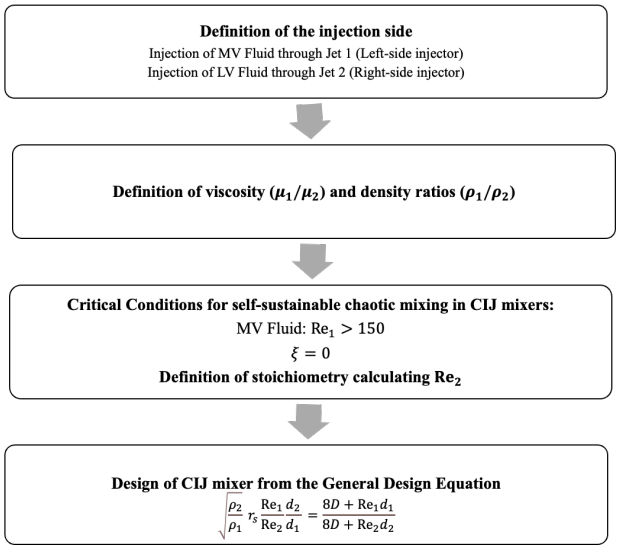

441

442 Figure 9. Flowchart for the design of experiments involving dissimilar fluids in CIJ mixers using the General
443 Design Equation.

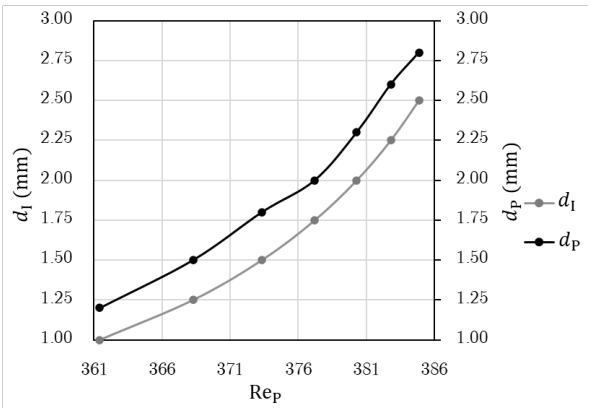


$r_s = 0.5$

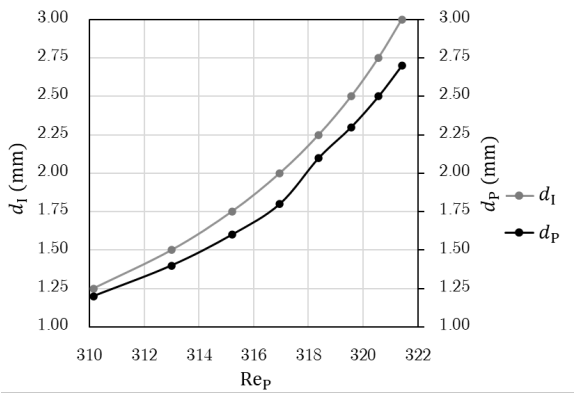


$r_s = 0.75$

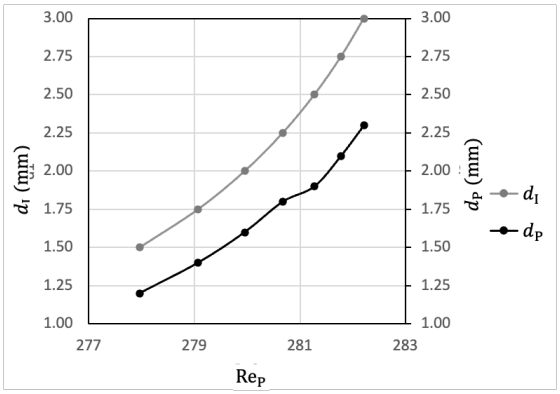


$r_s = 1$

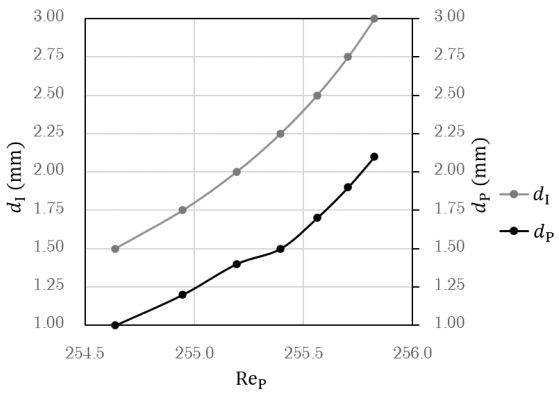


$r_s = 1.25$

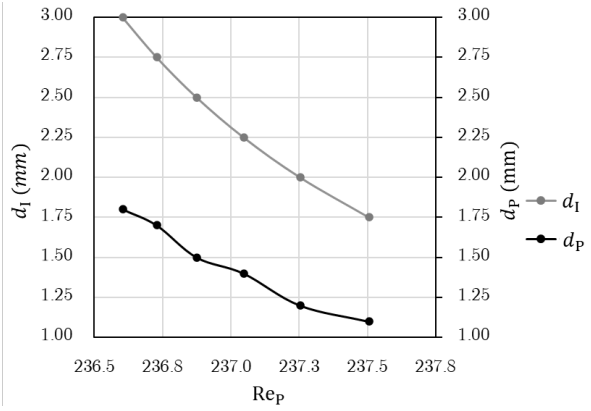


$r_s = 1.5$

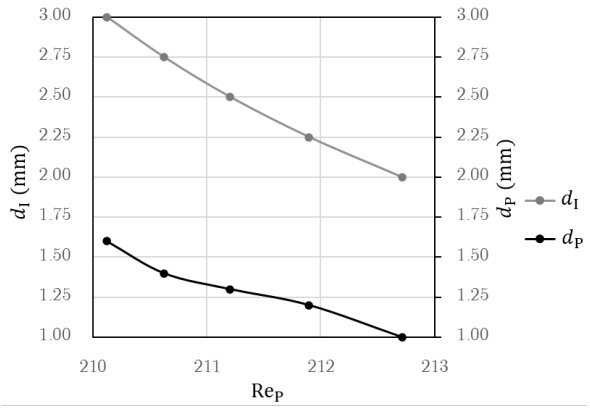


$r_s = 2$

Figure 10. Nozzle diameters for each stream ($d_P$ and $d_I$) in a typical range for RIM machines versus Reynolds number of polyol for different stoichiometric ratio $r_s = [0.5,2]$ and keeping constant the Reynolds number of isocyanate $\mathrm{Re} = 160$, where polyol has $\mu_\mathrm{P} = 0.6\ \mathrm{Pa \cdot s}$ and $\rho_\mathrm{P} = 900\ \mathrm{kg\ m^{-3}}$ and isocyanate has $\mu_\mathrm{I} = 0.2\ \mathrm{Pa \cdot s}$ and $\rho_\mathrm{I} = 1230\ \mathrm{kg\ m^{-3}}$.

## 5 Conclusions

Three models were considered here to predict the impingement point position in CIJ mixing chambers. The elastic analogue model, proposed by Fonte, Sultan et al. (2016), predicts the actual position of jets impingement point, from a spring analogy. The kinetic energy model predicts the collision of the two opposed jets from the balance of kinetic energy of two Lagrangian entities belonging to each liquid stream. The momentum model considers the balance of linear momentum of two entities inside of each fluid. Experimental and numerical results in Fonte, Sultan et al. (2016), Brito, Esteves et al. (2018) and Brito, Barbosa et al. (2022) were used to validate the range of application of each model. The three models account correctly for differences in the nozzles diameters. The elastic analogue model only predicts the impingement point position for mixing of similar fluids, i.e. fluids with the same viscosity and density. The momentum model has a validity range for fluids with a viscosity ratio from 1 to 9 and the same density (density ratio of approximately 1). The kinetic energy model, which is the basis for the General Design Equation of CIJs, has a broader range of applications since it predicts both mixing of similar fluids and fluids with quite different viscosity and density ratios. These results clearly show that the balance of two opposed jets is fully described by the balance of kinetic energy at the impingement point position.

Previous studies suggest that the mixing efficiency is obtained when the operation conditions and CIJ geometry ensure the impingement of both jets at mixing chamber axis, i.e. for the balance of jets. The definition of stoichiometry, the working conditions of the more viscous liquid stream $\mathrm{Re}_{\mathrm{MV}} > 150$, and the balance of jets enables further design of CIJ geometry from the implementation of the General Design Equation.

## 6 Acknowledgments

This work was financially supported by: LA/P/0045/2020 (ALiCE), UIDB/50020/2020 e UIDP/50020/2020 (LSRE-LCM), by national funds through FCT/MCTES (PIDDAC), by POCI-01-0145-FEDER-016851 and by POCI-01-0145-FEDER-030445 – funded by FEDER funds - Programa Operacional Competitividade e Internacionalização (POCI) – and by national funds through FCT -

Fundação para a Ciência e a Tecnologia I.P; Margarida S.C.A. Brito acknowledges her FCT scholarship PD/BD/135060/2017.

Margarida S.C.A. Brito and C. P. Fonte acknowledge financial support from the Department of Chemical Engineering and Analytical Science of the University of Manchester that enabled M.S.C.A. Brito's secondment in the UK.

## 7 References

Bird, R. B., et al. (2002). Transport Phenomena John Wiley & Sons.

Brito, M. S. C. A., et al. (2022). "Effective mixing of dissimilar fluids in asymmetric Confined Impinging Jets mixers." Chemical Engineering Science **258**: 117756.

Brito, M. S. C. A., et al. (2018). "Mixing of fluids with dissimilar viscosities in Confined Impinging Jets." Chemical Engineering Research and Design **134**: 392-404.

Erkoç, E., et al. (2007). "Mixing dynamics control in RIM machines." Chemical Engineering Science **62**(18): 5276-5281.

Fonte, C. P., et al. (2011). "Quantification of mixing in RIM using a non-diffusive two-phase flow numerical model." International Journal of Chemical Reactor Engineering **9**: A114.

Fonte, C. P., et al. (2015). "Flow imbalance and Reynolds number impact on mixing in Confined Impinging Jets." Chemical Engineering Journal **260**: 316-330.

Fonte, C. P., et al. (2016). "An elastic analog model for controlling the impingement point position in confined impinging jets." AIChE Journal **62**(6): 2200-2212.

Gavi, E., et al. (2007). "CFD modelling and scale-up of Confined Impinging Jet Reactors." Chemical Engineering Science **62**(8): 2228-2241.

Gavi, E., et al. (2008). "On the Importance of Mixing for the Production of Nanoparticles." Journal of Dispersion Science and Technology **29**(4): 548-554.

Gavi, E., et al. (2010). "Turbulent precipitation in micromixers: CFD simulation and flow field validation." Chemical Engineering Research and Design **88**(9): 1182-1193.

Gavi, E., et al. (2007). "CFD modelling of nano-particle precipitation in confined impinging jet reactors." Chemical Engineering Research and Design **85**(5 A): 735-744.

Gomes, N. M. O., et al. (2016). "Real time control of mixing in Reaction Injection Moulding." Chemical Engineering Research and Design **105**: 31-43.

Icardi, M., et al. (2011). "Investigation of the flow field in a three-dimensional Confined Impinging Jets Reactor by means of microPIV and DNS." Chemical Engineering Journal **166**(1): 294-305.

Johnson, D. A. (2000). "Experimental and Numerical Examination of Confined Laminar Opposed Jets. Part I Momentum Imbalance." International Communications in Heat and Mass Transfer **27**(4): 443-454.

Johnson, D. A. (2000). "Experimental and Numerical Examination of Confined Laminar Opposed Jets. Part II Momentum Balancing." International Communications in Heat and Mass Transfer **27**(4): 455-463.

Johnson, D. A., et al. (1996). "The Effect of Geometrical Parameters on the Flow Field of an Opposed Jet RIM Mix Head: Equal Flow and Matched Fluids." Canadian Journal of Chemical Engineering **74**(1): 40-48.

Keuerleber, R. and F. Pahl (1970). Device for feeding flowable material to a mold cavity.

Lee, L. J., et al. (1980). "Impingement mixing in reaction injection molding." Polymer Engineering & Science **20**(13): 868-874.

Li, W.-F., et al. (2013). "Experimental study of planar opposed jets with acoustic excitation." Physics of Fluids **25**(1): 014108.

Li, W. F., et al. (2016). "Experimental study about mixing characteristic and enhancement of T-jet reactor." Chemical Engineering Science **144**: 116-125.

Lince, F., et al. (2009). "Smart mixers and reactors for the production of pharmaceutical nanoparticles: Proof of concept." Chemical Engineering Research and Design **87**(4): 543-549.

Lopes, J. C. B., et al. (2013). Opposed jets mixing chamber for mixing of fluid with different mass fluxes, . WIP.

Malguarnera, S. C. and N. P. Suh (1977). "Liquid injection molding I. An investigation of impingement mixing." Polymer Engineering & Science **17**(2): 111-115.

Marchisio, D. L., et al. (2008). "Effect of Mixing and Other Operating Parameters in Sol−Gel Processes." Industrial & Engineering Chemistry Research **47**(19): 7202-7210.

554
555 Marchisio, D. L., et al. (2006). "Design and scale-up of chemical reactors for nanoparticle
556 precipitation." AIChE Journal **52**(5): 1877-1887.
557
558 Nakamura, S. and R. S. Brodkey (2000). Direct and Large Eddy Simulation of the Three-
559 Dimensional Unsteady Flows in the Counter-Jet Mixing Vessel. ASME Fluids Engineering
560 Summer Conference, Boston, Massachusetts.
561
562 Nunes, M. I., et al. (2012). "Micromixing assessment of confined impinging jet mixers used
563 in RIM." Chemical Engineering Science **74**: 276-286.
564
565 Ranz, W. E. (1986). "Analysis of reaction processes in which microscopic heterogeneities
566 appear: scale-up and scale-down of polymerization reactions." Industrial & Engineering
567 Chemistry Fundamentals **25**(4): 561-565.
568
569 Sandell, D. J., et al. (1983). "Visualization Tecnique For Studying Impingement Mixing at
570 Representative Reynolds Numbers." Polymer Process Engineering **3**(1-2): 57-70.
571
572 Santos, R. J., et al. (2009). "Dynamic behavior of the flow field in a RIM machine mixing
573 chamber." AIChE Journal **55**(6): 1338-1351.
574
575 Santos, R. J., et al. (2008). "Hydrodynamics of the mixing chamber in RIM: PIV flow-field
576 characterization." AIChE Journal **54**(5): 1153-1163.
577
578 Schütz, S., et al. (2005). "Charakterisierung des Mischverhaltens von Gegenstrom-Injektions-
579 Mischern." Chemie Ingenieur Technik **77**(4): 398-405.
580
581 Shi, Z.-h., et al. (2015). "Experimental study of mixing enhancement of viscous liquids in
582 confined impinging jets reactor at low jet Reynolds numbers." Chemical Engineering Science
583 **138**: 216-226.
584
585 Tucker, C. L. and N. P. Suh (1980). "Mixing for reaction injection molding II. Impingement
586 mixing of fiber suspensions." Polymer Engineering & Science **20**(13): 887-898.
587
588 Tucker, C. L. and N. P. Suh (1980). "Mixing for reaction injection molding. I. Impingement
589 mixing of liquids." **20**(13): 875-886.
590
591 Unger, D. R. and F. J. Muzzio (1999). "Laser-induced fluorescence technique for the
592 quantification of mixing in impinging jets." AIChE Journal **45**(12): 2477-2486.
593
594 Unger, D. R., et al. (1998). "Experimental and Numerical Characterization of Viscous Flow
595 and Mixing in an Impinging Jet Contactor." The Canadian Journal of Chemical Engineering
596 **76**: 546-555.

White, F. M. (2006). Viscous Fluid Flow, McGraw-Hill.

Wood, P., et al. (1991). "Experimental and computational studies of the fluid mechanics in an opposed jet mixing head." Physics of Fluids A **3**(5): 1362-1368.

Zhao, Y. and R. S. Brodkey (1998). "Averaged and Time-resolved Full-field (three-dimensional), Measurements of Unsteady Opposed Jets." The Canadian Journal of Chemical Engineering **76**: 536-545.

Zhao, Y. and R. S. Brodkey (1998). "Particle paths in three-dimensional flow fields as a means of study: Opposing jet mixing system." Powder Technology **100**(2): 161-165.